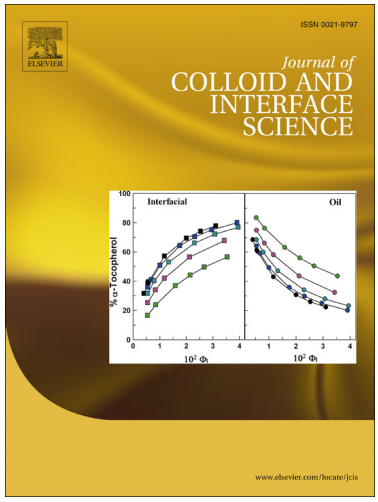

One-pot Hydrothermal Synthesis of $Co(OH)_2$ Nanoflakes on Graphene Sheets and Their Fast Catalytic Oxidation of Phenol in Liquid Phase

Yunjin Yao, Chuan Xu, Shiding Miao, Hongqi Sun, Shaobin Wang

PII: S0021-9797(13)00334-2
DOI: http://dx.doi.org/10.1016/j.jcis.2013.03.070
Reference: YJCIS 18736

To appear in: *Journal of Colloid and Interface Science*

Received Date: 31 January 2013
Accepted Date: 29 March 2013

Please cite this article as: Y. Yao, C. Xu, S. Miao, H. Sun, S. Wang, One-pot Hydrothermal Synthesis of $Co(OH)_2$ Nanoflakes on Graphene Sheets and Their Fast Catalytic Oxidation of Phenol in Liquid Phase, *Journal of Colloid and Interface Science* (2013), doi: http://dx.doi.org/10.1016/j.jcis.2013.03.070

One-pot Hydrothermal Synthesis of $Co(OH)_2$ Nanoflakes on Graphene Sheets and Their Fast Catalytic Oxidation of Phenol in Liquid Phase

Yunjin Yao[1,2*], Chuan Xu[1], Shiding Miao[1], Hongqi Sun[2], Shaobin Wang[2*]

[1]School of Chemical Engineering, Hefei University of Technology, Hefei 230009, China

[2]Department of Chemical Engineering, Curtin University, G.P.O. Box U1987, Perth, WA 6845, Australia

ABSTRACT: A cobalt hydroxide ($Co(OH)_2$) nanoflake-reduced graphene oxide (rGO) hybrid was synthesized by a one-pot hydrothermal method using glucose as a reducing agent for graphene oxide (GO) reduction. The structural and surface properties of the material were investigated by scanning and transmission electron microscopies, energy-dispersive X-ray spectrometry, powder X-ray diffraction, Fourier transform infrared spectroscopy, and thermogravimetric analysis. Catalytic activities of GO, rGO, $Co(OH)_2$ and $Co(OH)_2$–rGO in aqueous phenol degradation using peroxymonosulfate as an oxidant were compared. A synergetic effect on the catalytic activity was found on the $Co(OH)_2$–rGO hybrid. Although rGO has weak catalytic activity, $Co(OH)_2$-rGO hybrid showed a higher catalytic activity than $Co(OH)_2$. The phenol degradation on $Co(OH)_2$-rGO was extremely fast and took around 10 min for 100% phenol removal. The degradation was found to follow the first order kinetics and a mechanism for phenol degradation was presented.

KEYWORDS: Cobalt hydroxide; Graphene; Phenol; Catalytic oxidation; Water treatment

* To whom correspondence should be addressed:
Yunjin Yao; Phone: +86 551 2901458; Fax: +86 551 2901450; E-mail:yaoyunjin@gmail.com
Shaobin Wang; Phone: +61 8 9266 3776; Fax: +61 8 9266 2681; E-mail: shaobin.wang@cutin.edu.au

1. Introduction

Recently, cobalt hydroxide has attracted increasing attention due to its good electrochemical, optical and catalytic properties [1]. Generally, cobalt hydroxide presents in two polymorphic phases, α- and β-$Co(OH)_2$, which show a hexagonal layered structure. α-$Co(OH)_2$ presents as hydrotalcite-like structure, consisting of $Co(OH)_2$−x layers with positive charges balanced by inserted anions between the interlayers. β-$Co(OH)_2$ displays a brucite-like structure with a Co layer sandwiched by two O layers [2-4]. α-$Co(OH)_2$ usually has a larger interlayer spacing (>7.0 Å) than β-$Co(OH)_2$ (4.6 Å), making the α-$Co(OH)_2$ possessing a higher chemical activity. Cao et al. [5] prepared $Co(OH)_2$/Y-zeolite nanocomposites by coupling Co hydroxide to an ultrastable Y-type zeolite as supercapacitors with high energy density. Xia et al. [6] reported a novel 3D porous nano-Ni/$Co(OH)_2$ nanoflake composite as a film electrode for supercapacitors with both high power and energy capabilities. In such applications, α-$Co(OH)_2$ was found to be a promising material due to the interesting interlayer chemistry.

Graphene, a single- or multiple-layer of carbon material with a two-dimensional honeycomb sp^2 carbon lattice, possesses many unique features such as large surface area, good electrical, thermal, and mechanical properties [7-9]. Being an unrolled carbon nanotube, graphene has been a hot topic in view of its high specific area that can serve as a superior platform for building hybrids. Integration of nanoparticles, such as Fe_3O_4, MnO_2, TiO_2, Pt, Ag, etc., onto graphene sheets to make new hybrids will produce special features that can be widely utilized in catalysis, supercapacitors, Li-ion batteries, biomedical fields, etc. [10, 11]. The graphene favours better dispersion of nanoparticles and thus improves the catalytic activity and durability. A few investigations have been conducted in preparation of Co hydr(oxide)-graphene hybrids and their applications in electrochemistry as electrodes [2, 12-15]. He et al. [13] synthesized a β-$Co(OH)_2$-graphene composite for rechargeable lithium batteries. They found that the particular structure of β-$Co(OH)_2$ particles surrounded by the graphene sheets could limit the volume change during cycling and provided an excellent electronic conduction pathway. After 30 cycles, the reversible capacity of $Co(OH)_2$-graphene is still 910 mAh/g with the retention of 82%. Chen

et al. [16] reports a facile soft chemical approach to fabricate graphene-$Co(OH)_2$ nanocomposites in a water-isopropanol system using Na_2S as Co^{2+} depositing agent and graphite oxide reductant. Recently, Huang et al. [17] reported a complex process for self-assembled large-area $Co(OH)_2$ nanosheets/ionic liquid modified graphene heterostructures toward enhanced energy storage.

The presence of toxic organics in water is an important issue in water pollution. The cobaltous mediated homogeneous decomposition of peroxymonosulfate (Co/PMS) system for the degradation of organic contaminants has been proposed as a new process and demonstrated the advantages over Fenton reagent such as high efficiency in a wide pH range and small amounts of cobalt catalyst [18, 19]. Recently, several investigators have attempted using Co oxides [20, 21], and supported Co oxides [19, 22-24] as heterogeneous catalysts for activation of PMS to degrade organic pollutants. Although these catalysts are effective in initiating sulfate radical generation from PMS, low catalytic performance is still a major limitation for practical application in water treatment. Therefore, the search for new catalysts to activate PMS in high rate remains a main priority for the development of this technology. A few investigations have been conducted in preparation of $Co(OH)_2$-graphene hybrids and their applications in electrochemistry as electrodes, there is no report in $Co(OH)_2$ and $Co(OH)_2$-graphene hybrids as catalysts for activation of PMS.

In this study, we present a facile approach for the preparation of α-$Co(OH)_2$-reduced graphene oxide (rGO) hybrids using graphene oxide (GO) as a precursor for rGO, cobalt acetate tetrahydrate as a single sourced precursor of α-$Co(OH)_2$, and glucose as a reducing agent under hydrothermal conditions. The reducing ability of glucose is greatly enhanced for reduction of GO at hydrothermal conditions. $Co(OH)_2$ and $Co(OH)_2$–graphene hybrid were then tested in phenol degradation using PMS as an oxidant and shown the potential for phenol removal. The catalytic reaction kinetics of phenol degradation and mechanism were investigated.

2. Experimental

2.1 Materials

Graphite powder (99.9995%), D-(+)-glucose (99.5%), cobalt (II) acetate tetrahydrate, and potassium peroxymonosulfate ($2KHSO_5•3KHSO_4•3K_2SO_4$ available as Oxone, PMS) were obtained from Sigma-Aldrich, USA. Hydrogen peroxide (30 wt%) was purchased from Chem-Supply, Australia. Potassium permanganate, ammonia solution (28%) and phenol were obtained from Ajax Finechem, Australia. Hydrochloric acid (32%) was supplied from Biolab, Australia. All the chemicals were used as received without further purification.

2.2 Preparation of α-$Co(OH)_2$, rGO and α-$Co(OH)_2$-rGO

Graphene oxide (GO), prepared from natural graphite by the modified Hummer's method[25-27] which includes pre-oxidation of the graphite by concentrated H_2SO_4 and $KMnO_4$, re-oxidation with H_2O_2, and exfoliation by sonication, was used as the starting material for the fabrication of α-$Co(OH)_2$-rGO hybrids. A one-pot hydrothermal method was employed to produce α-$Co(OH)_2$-rGO hybrid. Firstly, 0.4 g of prepared GO was mixed with 300 mL of deionized water and underwent sonication for 120 min to get exfoliated GO. Next, 350 mg of cobalt acetate tetrahydrate ($Co(C_2H_3O_2)_2•4H_2O$) were added to the GO solution. Meanwhile, 10 mL $NH_3•H_2O$ and 0.32 g of glucose were added to the above solution simultaneously. Finally, the mixture was sealed in a 100 mL Teflon-lined autoclave, heated to 160 ℃, and maintained at the temperature for 4 h. The as-synthesized product (α-$Co(OH)_2$-rGO) was then collected by centrifugation, washed with pure water and ethanol several times, and dried at 80 ℃ for 12 h. Pure α-$Co(OH)_2$ and rGO were also obtained via the similar process in the absence of either GO or cobalt acetate, respectively. The synthesis process of the α-$Co(OH)_2$-rGO hybrid is schematically illustrated in Figure 1.

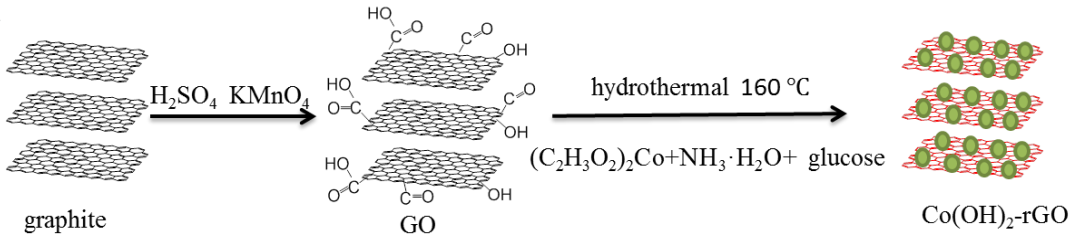

Figure 1 Synthesis route of α-$Co(OH)_2$-rGO.

2.3 Characterization

Morphologies of as-synthesized materials were observed from field emission scanning electron microscopy (FESEM , Zeiss Neon 40EsB FIBSEM) and transmission electron microscopy (TEM (JEOL 2011 TEM) equipped with energy-dispersive X-ray spectrometry (EDS). Powder X-ray diffraction (XRD) patterns of all samples were determined on a Bruker D8-Advance X-ray diffractometer with Cu Kα radiation (λ = 1.5418 Å), at accelerating voltage and current of 40 kV and 40 mA, respectively. Fourier transform infrared spectroscopy (FT-IR) spectra were obtained on a Perkin-Elmer Spectrum 100 with a resolution of 4 cm^{-1} in transmission mode at room temperature. Thermogravimetric and differential scanning calorimetry (TG-DSC) analysis was performed on a Perkin-Elmer Diamond TG/DTA thermal analyzer by heating the samples in an air flow of 100 mL/min and at a heating rate of 10 ºC/min. The BET surface areas of as-prepared samples were determined by N_2 adsorption on a Quantachrome NOVA 1200 Sorptomatic apparatus (USA) at -196 ºC. The specific surface areas were calculated using the BET equation.

2.4 Catalytic oxidation

The catalytic oxidation of phenol was carried out in a 500 mL reactor containing 30 mg/L of phenol solution. The reaction solution was stirred continuously to maintain homogeneous solution at ambient temperature (25±2 ºC). 0.25 g of PMS were added to the phenol solution and allowed to dissolve before the reaction. Later 10 mg of four different catalysts, GO, rGO, α-$Co(OH)_2$ and α-$Co(OH)_2$-rGO, were added in to start the reaction. At predetermined time intervals, 0.5 mL liquid was withdrawn into a HPLC vial using a syringe filter, and 0.5 mL of methanol was added to quench the reaction. The concentrations of phenol and intermediates were analyzed using a HPLC with a UV detector at the wavelength of 270 nm. The column used was C-18 and the mobile phase was a mixed solution of 30% CH_3CN and 70% water [28, 29].

3. Results and discussion

The adsorption surface areas of the synthesized materials were obtained by N_2 adsorption isotherms at values of 1.9 and 86.7 m^2/g for α-$Co(OH)_2$ and α-$Co(OH)_2$-rGO hybrid, respectively. Morphology and structure of the synthesized α-$Co(OH)_2$ are characterized by FESEM and TEM images (Figure 2). The as-synthesized $Co(OH)_2$ samples show in microsphere congregated randomly by pieces of nanoflakes (Figure 2a). The high magnification SEM image (Figure 2b) reveals that the thickness of each flake is about 5-10 nm. Such unique structure provides an important morphological basis helping to enlarging the contact area and enhancing the bulk accessibility of $Co(OH)_2$ for fast catalytic reactions. TEM measurements provide further insights into the morphology and structure of the $Co(OH)_2$ sample, as shown in Figure 2c. The TEM images are consistent with the FESEM images and confirm the size distribution at higher magnification. As illustrated in Figure 2d, the presence of α-$Co(OH)_2$ particles was further confirmed by EDS analysis. Apart from C and Cu peaks from the TEM grid, only Co and O were detected, indicating the structure of α-$Co(OH)_2$ particles.

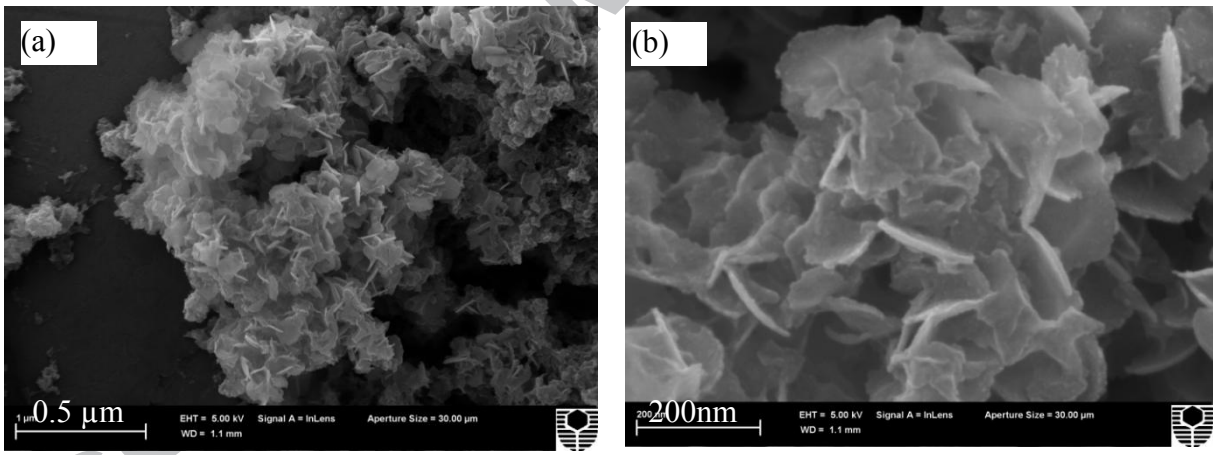

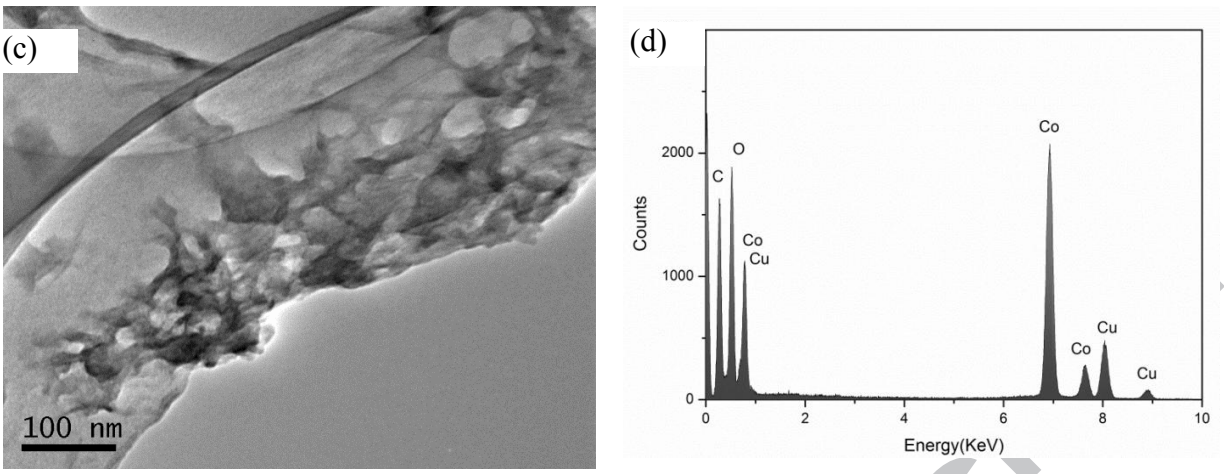

Figure 2 FESEM (a,b) and TEM (c) images of α-$Co(OH)_2$ and (d) EDS for α-$Co(OH)_2$.

Figure 3 shows typical FESEM and TEM images of as-prepared α-$Co(OH)_2$-rGO hybrid formed by reacting $Co(CH_3COO)_2$ with GO through the hydrothermal process. The graphene is clearly visible from the FESEM and TEM images shown in Figure 3a-d. Figure 3a shows that the α-$Co(OH)_2$ nanoflakes were dispersed on the basal planes of graphene, which is different from pure α-$Co(OH)_2$. From Figure 3b, it can also be observed that graphene sheets were distributed between the loosely packed α-$Co(OH)_2$ nanoflakes which prevented the aggregation of α-$Co(OH)_2$ nanoflakes to a certain extent. This can be of a great benefit to catalytic reactions. The TEM images (Figure 3c, d) reveal the similar features to the FESEM results. It is noted that the α-$Co(OH)_2$ nanoflakes are strongly anchored on the surface of the graphene sheets with a high density. This suggests a strong interaction between α-$Co(OH)_2$ nanoflakes and graphene sheets [30, 31]. As illustrated in Figure 3e, the presence of α-$Co(OH)_2$ nanoflakes was confirmed by EDS analysis.

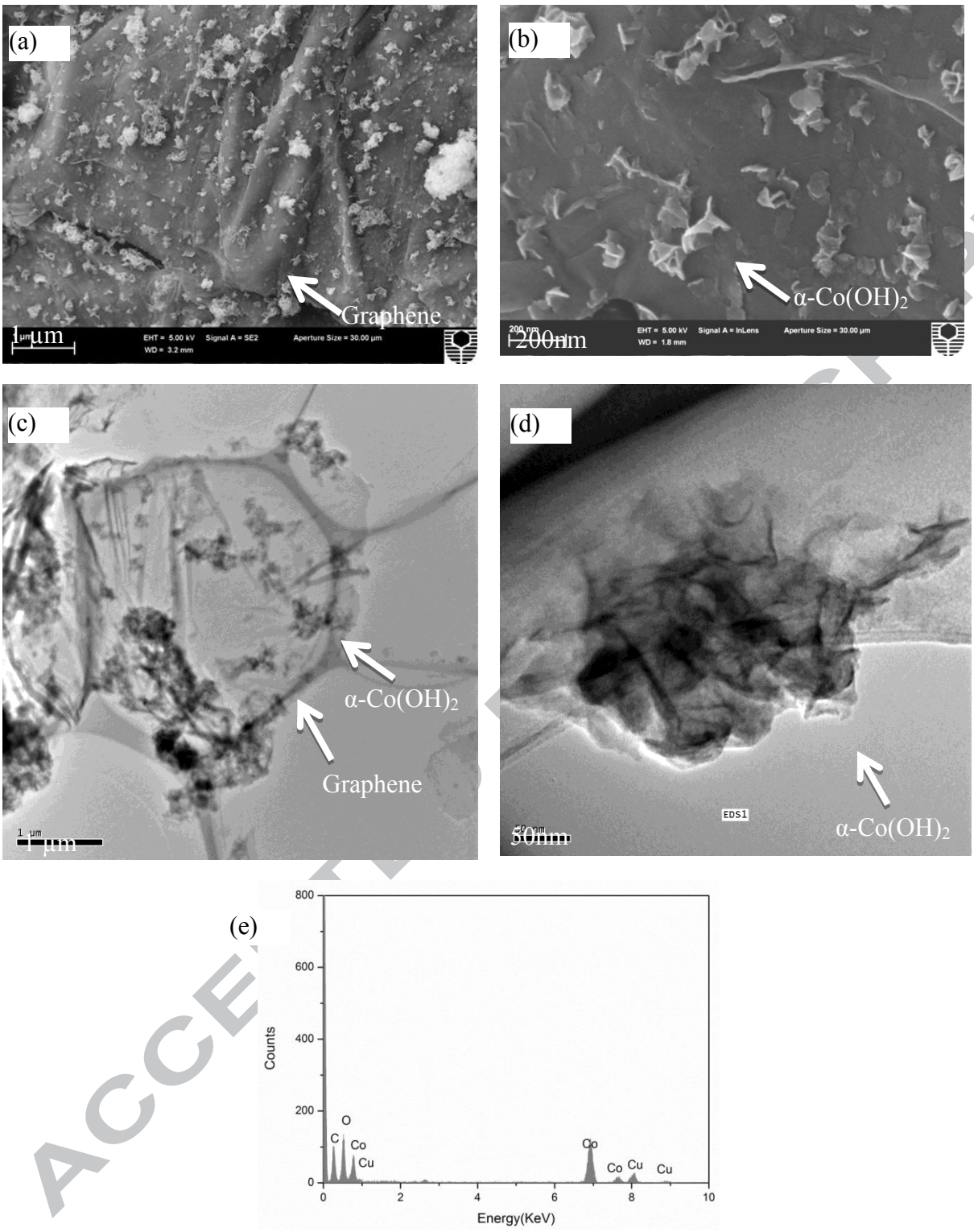

Figure 3 FESEM images (a: low-magnification, b: high-magnification), TEM (c: low-magnification, d: high-magnification), and (e) EDS for α-$Co(OH)_2$–rGO.

The crystalline structures of the prepared materials were further identified with XRD. The XRD patterns of GO, α-$Co(OH)_2$, and α-$Co(OH)_2$-rGO are shown in Figure 4a. The weak diffraction peaks at 9.2, 33.8 and 59.7° (curve b) are attributed to hydrotalcite α-$Co(OH)_2$ with a rhombohedra symmetry [1, 32, 33]. The low crystallinity and small crystallite sizes of the α-polymorph revealed by a considerable broadening of the peaks in the diffraction pattern could be due to some disorder of the layers oriented along the c-axis leading to a small number of parallel planes available for the diffraction. The same sets of characteristic peaks were also observed on α-$Co(OH)_2$-rGO. Furthermore, a very weak diffraction peak marked with a circle at 2θ=26° belongs to (001) of graphene. Compared to (002) diffraction peak of GO, the diffraction peak intensity of α-$Co(OH)_2$-rGO at 2θ=11° is obviously reduced, and XRD peak of GO (100) crystal at 2θ=42° totally disappears. These results suggest that the layered GO has been exfoliated largely, and more disordered stacking and less agglomeration of graphene sheets occurred in α-$Co(OH)_2$-rGO [34]. The XRD results indicate that exfoliated graphene sheets and hydrotalcite α-$Co(OH)_2$ nanoflakes coexist in the prepared hybrids.

FTIR spectra of GO, α-$Co(OH)_2$ and α-$Co(OH)_2$-rGO hybrids are shown in Figure 4b. In the spectrum of GO, C-H (2988 cm^{-1}), C=O (1713 cm^{-1}), aromatic C=C (1580 cm^{-1}), and alkoxy C-O (1043 cm^{-1}) stretching vibrations were observed. However, almost all the characteristic peaks of GO disappeared on α-$Co(OH)_2$-rGO samples after the hydrothermal reaction. Simultaneously, it could be clearly seen that a skeletal vibration absorption peak of graphene was appearing at about 1568 cm^{-1} [35], which confirms that GO was reduced to graphene in the presence of glucose. For α-$Co(OH)_2$, a broad band at about 3445 cm^{-1} is the stretching vibration of interlayer water molecules and of hydroxyl groups hydrogen-bonded to H_2O. The peaks at 1580 cm^{-1} and 1364 cm^{-1} can be attributed to the stretching -COO vibrations of free acetate ion [32].

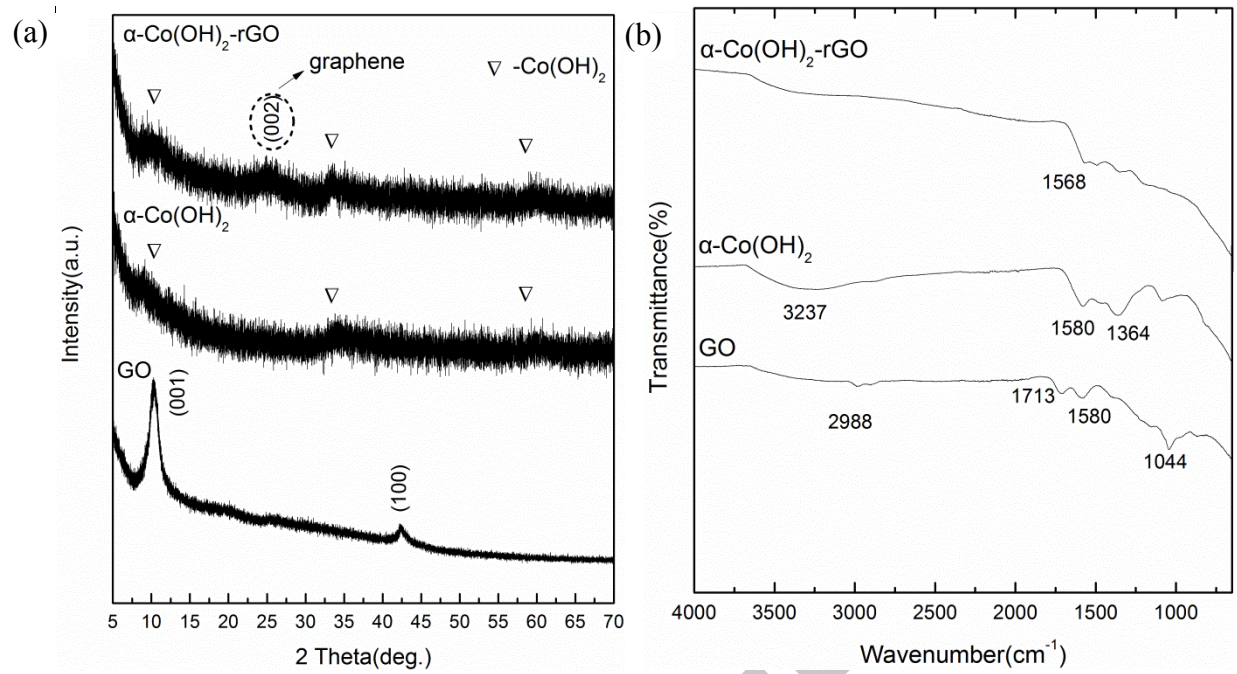

Figure 4 (a) XRD patterns and (b) FTIR spectra of GO, α-$Co(OH)_2$ and α-$Co(OH)_2$-rGO.

Thermal properties of GO, α-$Co(OH)_2$, and α-$Co(OH)_2$-rGO were investigated with TG-DSC. As shown in Figure 5a, GO is thermally unstable and shows three stages in weight loss. The weight loss below 150 ºC can be ascribed to the evaporation of surface adsorbed water molecules. The abrupt weight loss at 150 - 280 ºC can be assigned to the decomposition of the labile oxygen-containing functional groups to CO, CO_2, and H_2O [36]. Correspondingly, the DSC curve shows a strong exothermal peak centred at 200 ºC. The final peak of weight loss is occurring at 350 - 520 ºC and the DSC curve shows a much stronger exothermal peak centred at 516 ºC. It can be attributed to the oxidation of carbon skeleton [37]. The TG curve of α-$Co(OH)_2$ presents a strong weigh loss in the range of 200 to 330 ºC and the DSC curve shows a strong exothermal peak centred at 259 ºC. It suggests the decomposition of hydrotalcite-like structure of cobalt hydroxide to Co_3O_4[38]. In contrast to the results of GO and α-$Co(OH)_2$, TG curve of α-$Co(OH)_2$-rGO (Figure 5c) presents weight loss mainly in the range from 25 to 330 ºC. Correspondingly, the DSC curve shows three strong exothermal peaks centred at 227, 308 and 339 ºC, which are much lower than those occurring on GO and α-

$Co(OH)_2$. They can be assigned to the destruction of residual organic functional groups on graphene sheets, decomposition of hydrotalcite-like cobalt hydroxide and carbon skeleton combustion, respectively [37]. This weight change is similar to the results of carbon nanotube-cobalt systems and may be attributed to the catalytic role of $Co(OH)_2$ nanoflakes in oxidation of carbon materials [36, 39]. Based on the weight loss, $Co(OH)_2$ loading on α-$Co(OH)_2$-rGO is about 5 wt%. Nevertheless, the prepared materials are stable in air atmosphere at temperatures below 200 ºC and thus can be used in liquid phase reactions without concerns about their thermal stabilities.

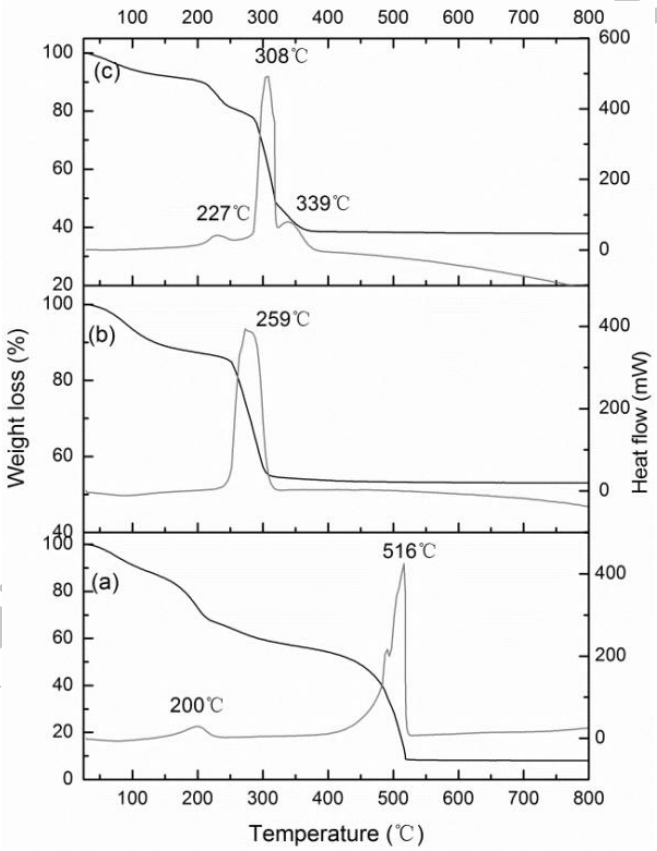

Figure 5 TG and DSC curves of (a) GO, (b) α-$Co(OH)_2$, (c) α-$Co(OH)_2$-rGO in air atmosphere.

To explore the catalytic applications, we investigated the catalytic performance of α-$Co(OH)_2$-rGO hybrid and individual components in catalytic oxidation of aqueous phenol in the presence of PMS (Figure 6a). Previous tests indicated that GO and rGO were able to adsorb phenol with low efficiency

[27, 40], which was negligible compared to the fast removal of phenol by heterogeneous catalytic reaction. For GO, little degradation of phenol could be observed in its catalytic reaction. However, nearly 11% of phenol was decomposed in 60 min for rGO, indicating rGO could activate PMS for minor phenol degradation, similar to the behavior of activated carbons [22]. The degradation rate of phenol on α-$Co(OH)_2$ or α-$Co(OH)_2$-rGO was much fast and complete phenol removal could be achieved around 60 min and 40 min, respectively. The phenol conversion was evaluated by the first-order kinetic model (Figure 6b) given in Eq.1.

$$\ln\left(\frac{C_t}{C_o}\right) = kt \qquad (1)$$

Where C_t and C_o are the phenol concentrations at time (t) and $t = 0$, respectively, and k is the rate constant. It is shown that phenol degradation on the both catalysts followed the first order kinetic model and phenol decomposition rates were considerably higher than those of the homogeneous Co^{2+} and oxide supported Co_3O_4 nanocatalysts reported in the literature (Table 1). α-$Co(OH)_2$-rGO hybrids exhibited better catalytic activity than pure α-$Co(OH)_2$, which can be attributed to several reasons. BET measurements showed that α-$Co(OH)_2$-rGO hybrids have a higher surface area (86.7 m^2/g) than α-$Co(OH)_2$ (1.9 m^2/g), resulting in more active sites for adsorption of phenol and its decomposition. SEM images demonstrated the high dispersion of α-$Co(OH)_2$ nanoflakes on α-$Co(OH)_2$-rGO hybrids. Reaction tests indicated that graphene is not only a support, but also a catalyst for oxidation of phenol. Thus, the novel properties of α-$Co(OH)_2$-rGO lead it as a promising catalyst and may also find application in other catalytic reactions.

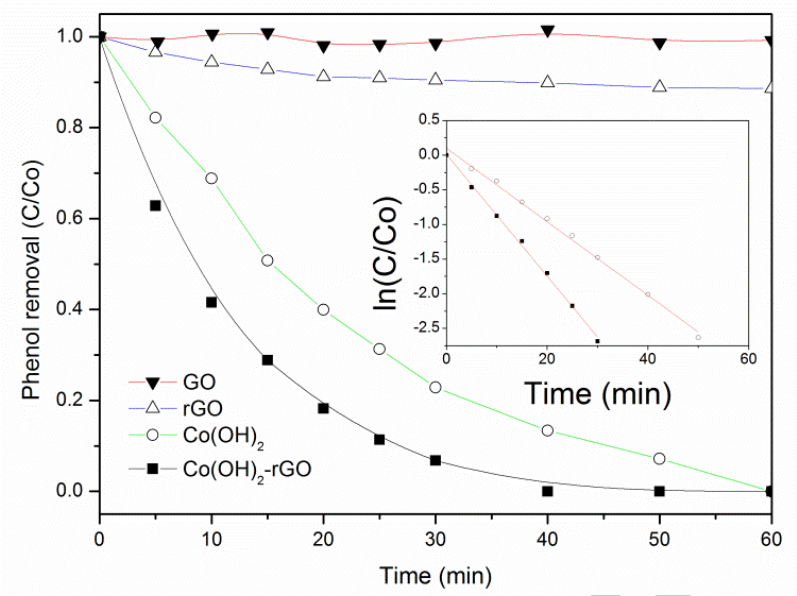

Figure 6 Phenol degradation in various Catalyst/PMS systems. Inset: kinetics of phenol degradation versus time. (Reaction conditions: [Phenol] = 30 mg/L, [PMS] = 0.5 g/L, [Catalyst] = 0.02 g/L)

[Table 1]

Some earlier studies reported the fundamentals of homogeneous cobalt-mediated activation of PMS for aqueous organics decomposition and it is believed that Co-OH^+ is active site for PMS activation for sulphate radical production [18, 41]. For a heterogeneous catalyst system, the general reaction mechanism may involve three steps, adsorption of phenol on solid catalyst surface, surface $Co(OH)_2$ particles reacting with PMS for sulphate radical generation, and the sulphate radical reacting with adsorbed or aqueous phenol eventually leading to the mineralization. In this investigation, three intermediates, 4-hydroxybenzoic acid, 1,2-dihydroxybenene, and *p*-benzoquinone were detected by HPLC in phenol degradation with α-$Co(OH)_2$/PMS or α-$Co(OH)_2$-rGO/PMS. Figure 7 shows the variations of intermediate concentration versus time during phenol degradation by α-$Co(OH)_2$/PMS or α-$Co(OH)_2$-rGO/PMS. For both catalyst systems, concentrations of 4-hydroxybenzoic acid and *p*-benzoquinone were generally higher than that of 1, 2-dihydroxybenene and being *p*-benzoquinone the

major intermediate. These results suggest that the reaction mechanism on the two catalysts is similar. It has been found that phenol degradation usually occurs from phenol hydroxylation in both *ortho* and *para* positions [42]. The concentration of intermediates indicated that hydroxylation of phenol predominantly occurs in the *para* position. Nevertheless, the intermediates still remained in the solution after phenol was completely decomposed. It is required more time for the reaction to be carried on to reach sufficiently low concentrations of intermediates, especially p-benzoquinone whose ecotoxicity is about three orders of magnitude higher than that of phenol itself. In addition, high oxidant amounts should be loaded in solution to reach complete degradation of organics. The reaction equations can be depicted as follows [43]:

$$Co(OH)_2 + HSO_5^- \rightarrow Co\text{-}OH^{2+} + SO_4^{-}\cdot + OH^- + H_2O \quad (2)$$

$$Co\text{-}OH^{2+} + HSO_5^- \rightarrow CoOH^+ + SO_5^{-}\cdot + H^+ \quad (3)$$

$$CoOH^+ + OH^- \rightarrow Co(OH)_2 \quad (4)$$

$$SO_4^{\bullet -} + \text{Phenol} \rightarrow [\text{...many steps...}] \rightarrow CO_2 + H_2O \quad (5)$$

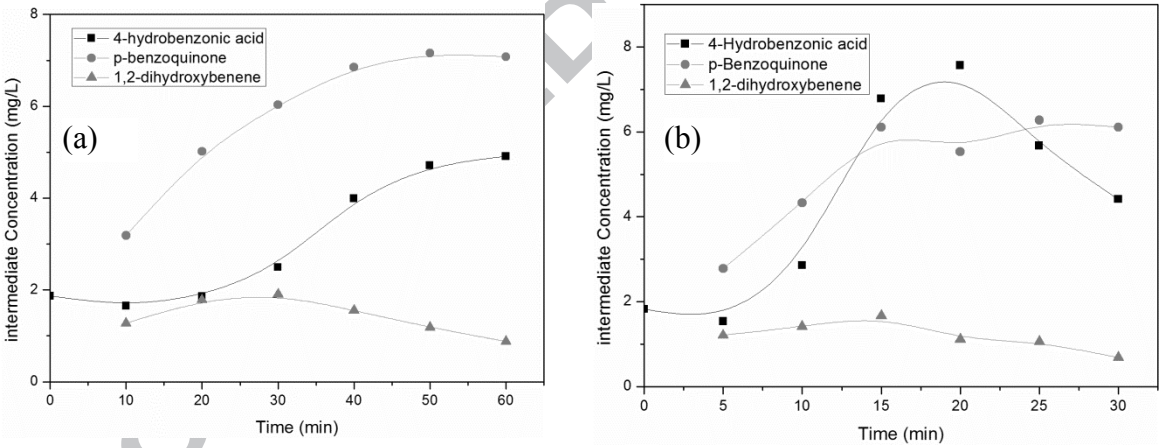

Figure 7 Variation of intermediate concentration from phenol transformation using (a) α-$Co(OH)_2$/PMS, and (b) α-$Co(OH)_2$-rGO/PMS (Reaction conditions: [Phenol] = 30 mg/L, [PMS] = 0.5 g/L,[Catalyst] = 0.02 g/L)

Further investigations showed that, upon increasing the α-$Co(OH)_2$-rGO catalyst dose from 10 to 50 mg, a faster and more efficient transformation of phenol occurred (Figure 8). Phenol degradation could be achieved in 10 min. The phenol removal efficiency is much higher than those of oxide supported Co_3O_4 catalysts [44] and similar to carbon supported Co_3O_4 systems [22, 27]. When the amount of catalyst in the solution is increased, the extent of active sites of α-$Co(OH)_2$ increases thereby resulting in an enhancement in generation of sulphate radicals, which in turn increases the rate of phenol oxidation. However, at high phenol concentration, removal efficiency would be decreased. For example, at phenol concentration of 100 mg/L, about 30% of phenol degradation was obtained within the same reaction time. In addition, in a sequential addition of phenol and PMS into the α-$Co(OH)_2$-rGO/PMS process, the degradation of phenol continued at a lower rate (Figure 8), due to the presence of intermediates. However, under sufficient supply of PMS, sulphate radicals would be generated and the reaction would be carried out until the target compound was completely removed. This suggested the potential of recycling α-$Co(OH)_2$-rGO in the process [18].

The occurrence of deactivation of α-$Co(OH)_2$-rGO is similar to all the heterogeneous Co catalysts reported. We have investigated the deactivation of heterogeneous Co catalysts and found that the catalyst deactivation would be attributed to three reasons: cobalt leaching, surface coverage of intermediates, and change in surface charges of catalysts [45]. The intermediate adsorption on catalyst surface plays a major role. Further investigation will be carried out to develop effective methods for α-$Co(OH)_2$-rGO catalyst regeneration.

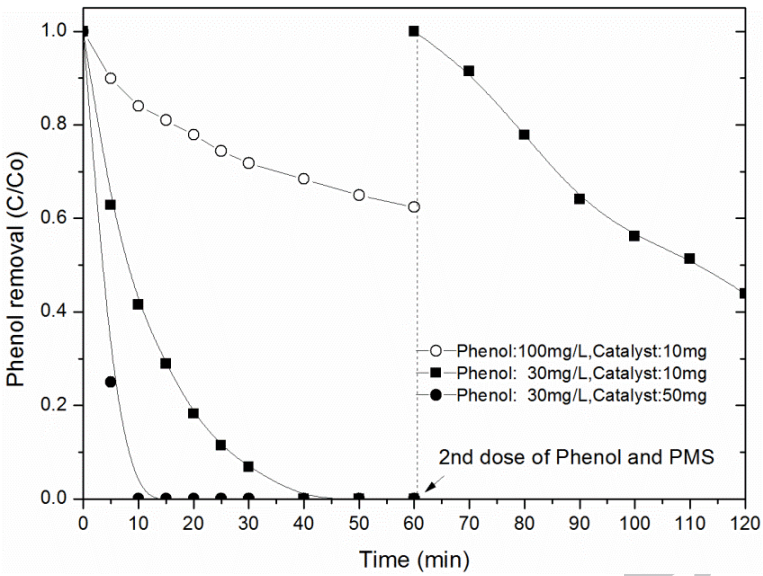

Figure 8 Phenol degradation in α-$Co(OH)_2$-rGO/PMS. (Reaction conditions: [PMS] = 0.5 g/L)

4. Conclusion

α-$Co(OH)_2$ nanoflake–rGO hybrids were successfully prepared by a one-pot hydrothermal method using graphene oxide, cobalt acetate, and glucose. Characterization by TEM, FESEM, EDS, XRD, FTIR and TG-DSC techniques showed that α-$Co(OH)_2$ nanoflakes were well dispersed on the basal planes of graphene. The α-$Co(OH)_2$-rGO exhibited much higher phenol degradation than graphene and α-$Co(OH)_2$. Phenol oxidation followed the first order kinetic model. The detection of intermediates indicated that phenol degradation occurred from hydroxylation predominantly in the *para* position.

Acknowledgments

This work was supported by supported by the Fundamental Research Funds for the Central Universities (NO. 2012HGQC0010) and the Anhui Provincial Natural Science Foundation (NO.1308085MB21).

References

[1] H. El-Batlouni, H. El-Rassy, M. Al-Ghoul, J. Phys. Chem. A 112 (2008) 7755.

[2] Z. Gui, J. Zhu, Y. Hu, Mater. Chem. Phys. 124 (2010) 243.

[3] A.D. Jagadale, V.S. Jamadade, S.N. Pusawale, C.D. Lokhande, Electrochimica Acta 78 (2012) 92.

[4] J.M. Ko, D. Soundarajan, J.H. Park, S.D. Yang, S.W. Kim, K.M. Kim, K.-H. Yu, Current Appl. Phys. 12 (2012) 341.

[5] L. Cao, F. Xu, Y.Y. Liang, H.L. Li, Adv. Mater. 16 (2004) 1853.

[6] X.H. Xia, J.P. Tu, Y.Q. Zhang, Y.J. Mai, X.L. Wang, C.D. Gu, X.B. Zhao, J. Phys. Chem. C 115 (2011) 22662.

[7] G. Eda, M. Chhowalla, Adv. Mater. 22 (2010) 2392.

[8] B.F. Machado, P. Serp, Catal. Sci. Technol. 2 (2012) 54.

[9] I.N. Kholmanov, S.H. Domingues, H. Chou, X. Wang, C. Tan, J.-Y. Kim, H. Li, R. Piner, A.J.G. Zarbin, R.S. Ruoff, ACS Nano 7 (2013) 1811.

[10] Y. Zhang, B. Chen, L. Zhang, J. Huang, F. Chen, Z. Yang, J. Yao, Z. Zhang, Nanoscale 3 (2011) 1446.

[11] S.D. Perera, R.G. Mariano, K. Vu, N. Nour, O. Seitz, Y. Chabal, K.J. Balkus, ACS Catal. 2 (2012) 949.

[12] J. Wu, D. Zhang, Y. Wang, Y. Wan, B. Hou, Journal of Power Sources 198 (2012) 122.

[13] Y.-S. He, D.-W. Bai, X. Yang, J. Chen, X.-Z. Liao, Z.-F. Ma, Electrochem. Commun. 12 (2010) 570.

[14] J. Zhu, Y.K. Sharma, Z. Zeng, X. Zhang, M. Srinivasan, S. Mhaisalkar, H. Zhang, H.H. Hng, Q. Yan, J. Phys. Chem. C 115 (2011) 8400.

[15] C. Nethravathi, M. Rajamathi, N. Ravishankar, L. Basit, C. Felser, Carbon 48 (2010) 4343.

[16] S. Chen, J. Zhu, X. Wang, J. Phys. Chem. C 114 (2010) 11829.

[17] X.-l. Huang, J. Chai, T. Jiang, Y.-J. Wei, G. Chen, W.-Q. Liu, D. Han, L. Niu, L. Wang, X.-B. Zhang, J. Mater. Chem. 22 (2012) 3404.

[18] K.H. Chan, W. Chu, Water Res. 43 (2009) 2513.

[19] P. Shukla, H. Sun, S. Wang, H.M. Ang, M.O. Tadé, Catal. Today 175 (2011) 380.

[20] G.P. Anipsitakis, E. Stathatos, D.D. Dionysiou, J. Phys. Chem. B 109 (2005) 13052.

[21] X. Chen, J. Chen, X. Qiao, D. Wang, X. Cai, Appl. Catal. B 80 (2008) 116.

[22] P.R. Shukla, S. Wang, H. Sun, H.M. Ang, M. Tadé, Appl. Catal. B 100 (2010) 529.

[23] Y. Ding, L. Zhu, A. Huang, Catal. Sci. Technol. 2 (2012) 1977.

[24] S. Muhammad, E. Saputra, H. Sun, J.d.C. Izidoro, D.A. Fungaro, H.M. Ang, M.O. Tade, S. Wang, RSC Adv. 2 (2012) 5645.

[25] T. Hartono, S. Wang, Q. Ma, Z. Zhu, J. Colloid Interface Sci. 333 (2009) 114.

[26] D.C. Marcano, D.V. Kosynkin, J.M. Berlin, A. Sinitskii, Z. Sun, A. Slesarev, L.B. Alemany, W. Lu, J.M. Tour, ACS Nano 4 (2010) 4806.

[27] Y. Yao, Z. Yang, D. Zhang, W. Peng, H. Sun, S. Wang, Ind. Eng. Chem. Res. 51 (2012) 6044.

[28] Y. Hardjono, H. Sun, H. Tian, C.E. Buckley, S. Wang, Chem. Eng. J. 174 (2011) 376.

[29] H. Sun, H. Tian, Y. Hardjono, C.E. Buckley, S. Wang, Catal. Today 186 (2012) 63.

[30] P. Lian, X. Zhu, H. Xiang, Z. Li, W. Yang, H. Wang, Electrochimica Acta 56 (2010) 834.

[31] G. Wang, T. Liu, X. Xie, Z. Ren, J. Bai, H. Wang, Mater. Chem. Phys. 128 (2011) 336.

[32] L. Kelpšaitė, J. Baltrušaitis, E. Valatka, Materials Science-Medziagotyra 17 (2011) 236.

[33] L.-X. Yang, Y.-J. Zhu, L. Li, L. Zhang, H. Tong, W.-W. Wang, G.-F. Cheng, J.-F. Zhu, Europ. J. Inorg. Chem. 2006 (2006) 4787.

[34] Z.-S. Wu, W. Ren, L. Wen, L. Gao, J. Zhao, Z. Chen, G. Zhou, F. Li, H.-M. Cheng, ACS Nano 4 (2010) 3187.

[35] S. Pan, X. Liu, X. Wang, Materials Characterization 62 (2011) 1094.

[36] C. Xu, X. Wang, J. Zhu, X. Yang, L. Lu, J. Mater. Chem. 18 (2008) 5625.

[37] J. Wang, S. Zheng, Y. Shao, J. Liu, Z. Xu, D. Zhu, J. Colloid Interface Sci. 349 (2010) 293.

[38] J. Yang, H. Liu, W.N. Martens, R.L. Frost, J. Phys. Chem. C 114 (2009) 111.

[39] J. Li, S. Tang, L. Lu, H.C. Zeng, J. Am. Chem. Soc. 129 (2007) 9401.

[40] H. Sun, S. Liu, G. Zhou, H.M. Ang, M.O. Tadé, S. Wang, ACS Appl. Mater. & Interfaces 4 (2012) 5466.

[41] G.P. Anipsitakis, D.D. Dionysiou, Environ. Sci. Technol. 37 (2003) 4790.

[42] J.A. Zazo, J.A. Casas, A.F. Mohedano, J.J. Rodríguez, Appl. Catal. B 65 (2006) 261.

[43] G.P. Anipsitakis, D.D. Dionysiou, M.A. Gonzalez, Environ. Sci. Technol. 40 (2006) 1000.

[44] P. Shukla, H.Q. Sun, S.B. Wang, H.M. Ang, M.O. Tade, Sep. Purif. Technol. 77 (2011) 230.

[45] H. Sun, H. Liang, G. Zhou, S. Wang, J. Colloid Interface Sci. 394 (2013) 394.

[46] Y. Yao, Z. Yang, H. Sun, S. Wang, Ind. Eng. Chem. Res. 51 (2012) 14958.

[47] E. Saputra, S. Muhammad, H. Sun, H.M. Ang, M.O. Tadé, S. Wang, Catal. Today 190 (2012) 68.

Figure captions

Figure 1 Synthesis route of α-$Co(OH)_2$-rGO.

Figure 2 FESEM (a,b) and TEM (c) images of α-$Co(OH)_2$ and (d) EDS for α-$Co(OH)_2$.

Figure 3 FESEM images (a: low-magnification, b: high-magnification), TEM (c: low-magnification, d: high-magnification), and (e) EDS for α-$Co(OH)_2$–rGO.

Figure 4 (a) XRD patterns and (b) FTIR spectra of GO, α-$Co(OH)_2$ and α-$Co(OH)_2$-rGO.

Figure 5 TG and DSC curves of (a) GO, (b) α-$Co(OH)_2$, (c) α-$Co(OH)_2$-rGO in air atmosphere.

Figure 6 Phenol degradation in various Catalyst/PMS systems. Inset: kinetics of phenol degradation versus time. (Reaction conditions: [Phenol] = 30 mg/L, [PMS] = 0.5 g/L, [Catalyst] = 0.02 g/L)

Figure 7 Variation of intermediate concentration from phenol transformation using (a) α-$Co(OH)_2$/PMS, and (b) α-$Co(OH)_2$-rGO/PMS (Reaction conditions: [Phenol] = 30 mg/L, [PMS] = 0.5 g/L,[Catalyst] = 0.02 g/L)

Figure 8 Phenol degradation in α-$Co(OH)_2$-rGO/PMS. (Reaction conditions: [PMS] = 0.5 g/L)

Table 1 Kinetic parameters of phenol degradation under α-$Co(OH)_2$/PMS and α-$Co(OH)_2$-rGO/PMS.

Catalyst	BET surface area (m^2/g)	Rate constant (k, min^{-1})	Regression coefficient (R^2)	Reference
α-$Co(OH)_2$	1.9	0.0530	0.995	This work
α-$Co(OH)_2$-rGO	86.7	0.0879	0.997	This work
Co_3O_4/rGO	-	0.100	0.982	[46]
Co_3O_4/AC	-	0.125	0.991	[22]
Co_3O_4/CA	-	0.0289	0.992	[28]
Co_3O_4/SBA-15	-	0.0741	0.994	[44]
Co_3O_4/Red-mud	-	0.0428	0.968	[47]
Co_3O_4/Fly-ash	-	0.00513	0.980	[47]
Co^{2+}	-	0.0830	0.993	[28]

Research Highlights

- $Co(OH)_2$-reduced graphene oxide (rGO) was synthesized by a one-pot hydrothermal method.
- Phenol degradation rate of $Co(OH)_2$-rGO using peroxymonosulfate was faster than $Co(OH)_2$.
- Kinetics of phenol degradation on $Co(OH)_2$–rGO follows a first-order model.
- A mechanism for phenol degradation was presented.

Graphical Abstract

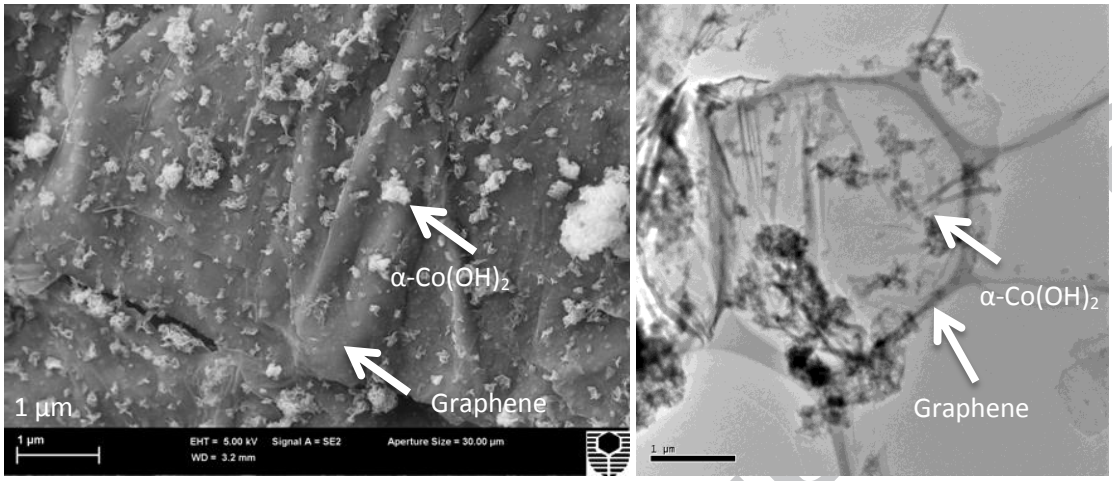

Catalytic Oxidation of Phenol